Eur. Phys. J. D **17**, 297–305 (2001)

THE EUROPEAN PHYSICAL JOURNAL D

EDP Sciences

Ionization of iridium ions in the Dresden EBIT studied by X-ray spectroscopy of direct excitation and radiative recombination processes

U. Kentsch[1], T. Werner[1], G. Zschornack[1,a], F. Grossmann[2], V.P. Ovsyannikov[2,b], and F. Ullmann[2]

[1] Technische Universität Dresden, Institut für Kern- und Teilchenphysik, Mommsenstr. 13, 01069 Dresden, Germany
[2] Leybold Vakuum Dresden GmbH, Zur Wetterwarte 50, 01109 Dresden, Germany

Received 12 July 2001 and Received in final form 10 September 2001

Abstract. Ir^{q+} $(41 \leq q \leq 64)$ ions with open-shell configurations have been produced in the electron beam of the room-temperature Dresden Electron Beam Ion Trap (Dresden EBIT) at electron excitation energies from 2 keV to 13 keV. X-ray emission from direct excitation processes and radiative capture in krypton-like to aluminium-like iridium ions is measured with an energy dispersive Si(Li) detector. The detected X-ray lines are analyzed and compared with results from multiconfigurational Dirac-Fock (MCDF) atomic structure calculations. This allows to determine dominant produced ion charge states at different electron energies. The analysis shows that at the realized working gas pressure of 5×10^{-9} mbar for higher charged ions the maximum ion charge state is not preferently determined by the chosen electron beam energy needed for ionization of certain atomic substates, but by the balance between ionization and charge state reducing processes as charge exchange and radiative recombination. This behaviour is also discussed on the basis of model calculations for the resulting ion charge state distribution.

PACS. 32.30.Rj X-ray spectra – 78.70.En X-ray emission spectra and fluorescence – 29.25.Ni Ion sources: positive and negative

1 Introduction

For the production of highly charged ions and their investigation by X-ray spectroscopy EBIT devices are a powerful tool and available yet at different laboratories. Up to now known working devices are preferently based on cryogenic techniques for the production of the magnetic fields with super-conducting Helmholtz coils focusing the electron beam to high electron beam densities. Basing on this working principle we have developed an EBIT working without any cryogenic techniques by substituting the super-conducting coils by permanent magnets (Dresden EBIT; [1–5]). Beside an excellent long-term stability the small dimensions of the room-temperature Dresden EBIT favorize it for spectroscopic investigations because of the possibility to realize relatively great solid angles that allows to reach sufficient count statistics at relatively low measurement times.

X-ray spectra of highly charged ions are of basic interest for investigations of the structure of multielectron systems in strong coulomb fields. Spectroscopic X-ray investigations of slow highly charged heavy ions are known predominantly from experiments realized at EBIT, as for instance investigations on tungsten [6], lead [7], thorium [8] and uranium [9]. In [10] the authors report on X-ray spectra emitted from highly ionized uranium from a laser-produced plasma. Wavelength dispersive measurements of X-ray transitions in highly charged neon-like ions are known from investigations performed at the Princeton Large Torus tokamak [11].

The aim of the present paper is the investigation of X-ray emission from different charged iridium ions by energy dispersive X-ray spectroscopy presenting spectra of krypton-like up to silicon-like ions including contributions from direct excitation and radiative recombination processes. We report on spectroscopic measurements on iridium ions in the electron energy region between 2 keV and 13 keV. Varying the electron beam energy spectra structures disappear and new structures arise. Continuously spectra are shifted in X-ray energies. L and M direct excitation and radiative recombination processes are studied. Further on dielectronic recombination processes can be observed at certain electron energy ranges. Together with results from multiconfigurational Dirac-Fock atomic

[a] e-mail: zschornack@physik.tu-dresden.de
[b] *Permanent address:* Joint Institute for Nuclear Research, LHE, Dubna, Russia.

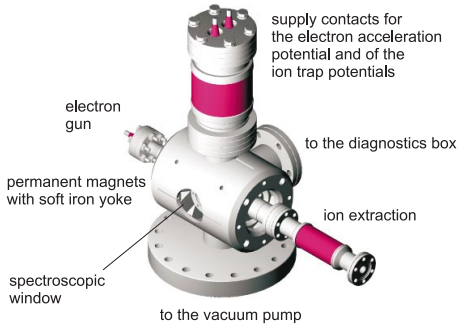

Fig. 1. 3D representation of the Dresden EBIT.

structure calculations the energetic signature of measured lines allows to determine ion charge states with a high level of confidence. Ion charge states determined that way are compared with modeling results for the ionization process in the Dresden EBIT where a satisfying correspondence is found.

To our knowledge iridium X-ray emission from highly charged ions has not yet been investigated experimentally. At the Dresden EBIT device iridium can be produced easily using a metal alloy cathode containing iridium. We measured iridium X-ray reference spectra at different excitation conditions with a Si(Li) solid state detector. Calculated X-ray energies give additional information on the spectra structure, *i.e.* the energetic behaviour of X-ray emission from different ion charge states.

The use of a room-temperature EBIT allows to investigate ionization processes in the electron beam in a wide range of working pressures from about 10^{-8} mbar up to 10^{-10} mbar. The results discussed in the present paper are derived at an operation pressure of 5×10^{-9} mbar. This pressure is significantly higher than the pressure characteristic at cryogenic EBIT operation.

2 Experimental setup

The measurements are realized at the Dresden EBIT. A 3D-representation of this device is shown in Figure 1. The basic function principle of the Dresden EBIT is to form a high dense electron beam by a specially designed electron gun with a high emissive metal alloy cathode which is containing iridium. The electron beam is compressed by the magnetic field of two permanent magnet rings. The ion trap where the ionization occurs is formed by a drift tube section ensemble. The high voltage of the central section accelerates the electrons to their final kinetic energy where the adjacent sections have an electric potential forming an electrostatic ion trap. The strongly compressed and accelerated energy-tunable monoenergetic electron beam produces, confines and excites highly charged ions which are localized in the beam. The most reachable ion charge state is defined by the voltage applied to the center drift tube and by the actual vacuum pressure, *i.e.* by the balance between electron impact ionization processes and contributions decreasing the ion charge state as charge exchange processes and radiative recombination. The actual main Dresden EBIT parameters used in the experiment are summarized in Table 1.

Table 1. Main Dresden EBIT parameters used in the experiment.

electron energy	2 keV – 13 keV
electron beam current	up to 40 mA
electron beam current density	(200...500) A cm^{-2}
vacuum with electron beam	5×10^{-9} mbar
ionization factor	(2...5) $\times 10^{21}$ cm^{-2}

As shown in Figure 1 the Dresden EBIT is equipped with a spectroscopic observation port with a spectroscopic window of 75 μm thick Be-foil. The distance between the Si(Li) solid state detector (resolution 133 eV at 6 keV X-ray energy) and the electron beam has been 47 mm where the minimum distance from the center of the electron beam to the vacuum window is 37 mm resulting in a solid angle of about 7×10^{-4}. All spectra are corrected for corresponding X-ray attenuation and detector efficiency.

Due to the construction and the working principle of the device the actual working pressure in the drift tube sections cannot be measured directly. Hence the indicated gas pressure can deviate from the actual pressure. Particle bombardment on inner tube walls can lead to desorption of gas molecules from the walls, *i.e.* the pressure inside the drift tubes can increase locally.

3 Iridium M-series X-ray emission

One of the most important advantages of an EBIT device is the capability to study selectively individual ions at different charge stages at different excitation conditions, *i.e.* at different electron energies. In the present paper we survey X-ray emissions from iridium ions over a wide range of ion charge states. In the X-ray energy region of iridium M-transitions the spectra become more complicated because they are generated from many different processes. Main contributions to the observed fluorescence spectra are radiative recombination (RR), dielectronic recombination (DR), direct excitation with following radiative decay (DE) and radiative cascades (RC). Contributions from electron bremsstrahlung processes are superimposed to the discrete X-ray lines resulting in a smooth background spectrum. It is not the aim of the present paper to investigate all the mentioned contributions in detail, but we discuss typical X-ray spectra derived at different excitation energies for highly charged iridium ions. We also note, that a change in source operation conditions (*e.g.* the pressure inside the trap or electron energy) can lead to significant changes in the form of the observed spectra.

In the investigated electron beam energy region direct excitation processes (DE) in iridium ions dominate. All DE processes show a threshold behaviour, *i.e.* X-ray spectra could change significantly at different electron energies. This concerns the appearance of different X-ray lines

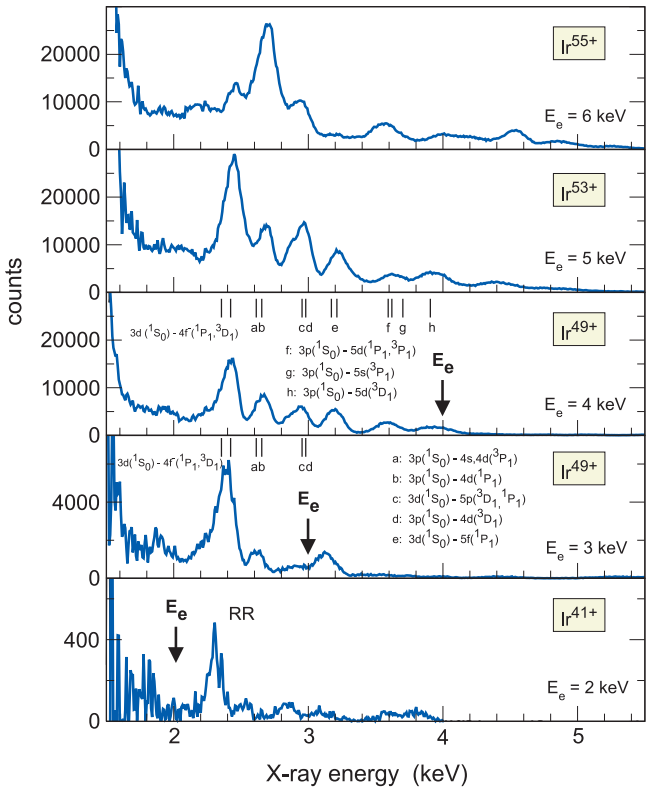

Fig. 2. Iridium excitation M X-ray lines at electron energies between 2 keV and 7 keV. All spectra are measured over the same time (2000 s) and under nearly equivalent vacuum conditions (5×10^{-9} mbar). Excitation channels are labeled. Electron beam energies are indicated by arrows.

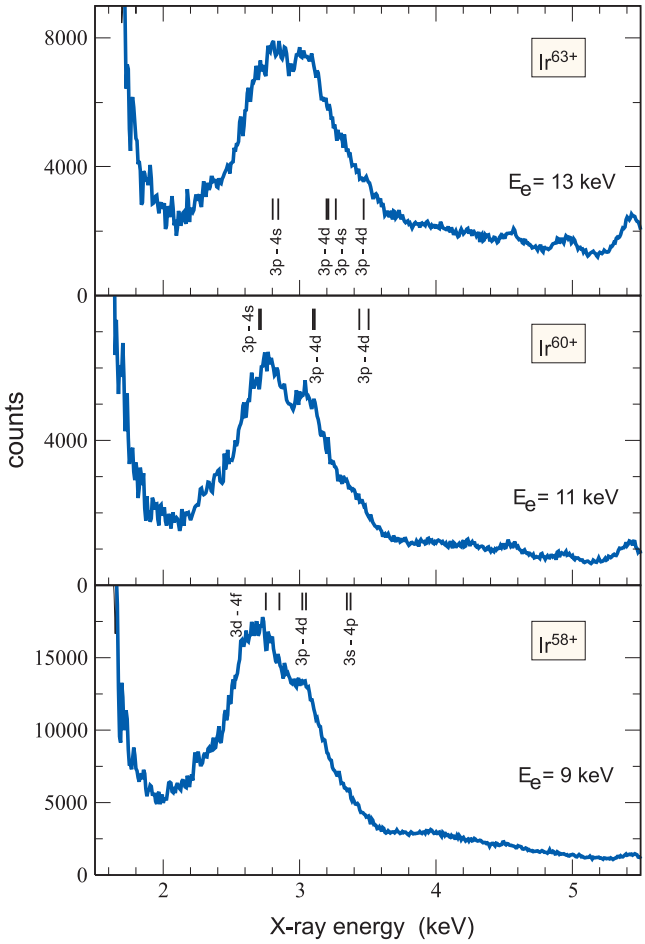

Fig. 3. Iridium excitation M X-ray lines at electron energies of 9 keV, 11 keV and 13 keV. All spectra are measured over the same time (2000 s) and under nearly equivalent vacuum conditions (5×10^{-9} mbar).

at different energetic positions as well as their intensity. In Figures 2 and 3 X-ray spectra for different excitation energies are shown where the indicated pressure was about 5×10^{-9} mbar as for all other spectra, too. As mentioned above the pressure is measured outside the drift tube ensemble, the actual pressure in the trap region can differ.

The observed X-ray spectra are a blend of lines emitted from ions with different charge states. Thereby the mean ion charge state arises with increasing excitation energy because higher electron energies allow to ionize deeper ion subshells. Calculated ionization energies of different iridium subshells for high ion charge states are listed in Table 2. The given values are extended average level (EAL) calculations performed with the GRASP-code [12]. From Table 2 it can be read that at electron energies of 4 keV the highest detectable ionization stage can be Ir^{49+}. For $E_e = 10$ keV it is possible to produce Ir^{67+}. At higher electron beam energies we observe ionization stages somewhat lower due to charge exchange and radiative recombination processes inside the trap.

Different formed spectra at different electron beam energies can be explained by the actual derived ion charge state distribution resulting in a close spectral overlap of X-ray emissions from ions of adjoining charge states. The increasing mean ionization stage appears in Figures 2 and 3 in an energy shift of X-ray lines to the high energy side of the spectra. In Figure 4 a X-ray spectrum at $E_e = 4$ keV is shown for the energy transition region of direct excitation lines decaying from $n = 4$, 5 shells into $n = 3$. The dominant ions here are nickel-like ions. Corresponding strong transitions are labeled according to the line positions and transition rates. The reached ionization stage corresponds to the highest ionization stage which is possible considering the electron ionization energies (see Tab. 2). This means, that at an energy of $E_e = 4$ keV ionization processes dominate.

In Figure 5 a calculated ion charge state distribution is shown where characteristic EBIT operation conditions are taken into account for the spectrum presented in Figure 4. The calculation is performed with a computer code described in [13] using a model which considers the important basic atomic processes as ionization, charge exchange and radiative recombination as well as occurring cooling processes and ion losses from the trap. The ion charge state distribution shown in Figure 5 can be characterized by predominantly contributions from Ir^{48+} and Ir^{49+} ions. The presence of a strong Ir^{48+} component can be explained by the role of radiative recombination.

Table 2. Electron ionization energies of iridium ions for different (nl) subshells at ion charge states q.

q	$1s$	$2s$	$2p$	$3s$	$3p$	$3d$	$4s$	$4p$
76	88115							
75	86441							
74	85869	21557						
73	85465	21200						
72	84904	20823	20649					
71	84279	20502	20213					
70	83766	20144	18124					
69	83272	19813	17772					
68	82796	19507	17390					
67	82337	19226	17045					
66	82116	19043	16861	7851				
65	81916	18881	16686	7711				
64	81691	18692	16494	7567	7422			
63	81452	18506	16305	7451	7273			
62	81242	18329	16121	7313	6709			
61	81038	18155	15947	7188	6580			
60	80839	17984	15774	7073	6441			
59	80645	17816	15616	6967	6315			
58	80449	17624	15413	6825	6160			
57	80254	17437	15232	6687	6032			
56	80061	17252	15043	6551	5896	5608		
55	79868	17074	14864	6423	5768	5465		
54	79685	16893	14678	6285	5628	5229		
53	79505	16718	14501	6153	5497	5092		
52	79327	16547	14329	6025	5369	4952		
51	79152	16380	14163	5900	5247	4805		
50	78980	16217	14003	5778	5131	4668		
49	78811	16057	13852	5658	5027	4540		
48	78711	15968	13762	5578	4947	4459	2721	
47	78618	15884	13675	5506	4871	4380	2656	
46	78520	15794	13585	5426	4792	4299	2591	2500
45	78419	15706	13496	5349	4715	4220	2538	2435
44	78327	15622	13410	5274	4639	4143	2476	2258
43	78237	15539	13327	5200	4566	4069	2420	2201
42	78149	15458	13245	5128	4494	3996	2368	2139
41	78063	15378	13168	5057	4427	3923	2321	2083

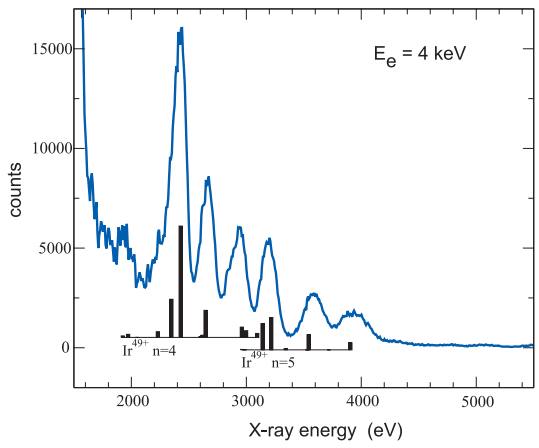

Fig. 4. Iridium excitation M X-ray lines at an electron energy of 4 keV with predominantly nickel-like iridium ions. For excitation processes to $n = 4$ and $n = 5$ energetic positions and transition rates of the strongest transition lines are indicated.

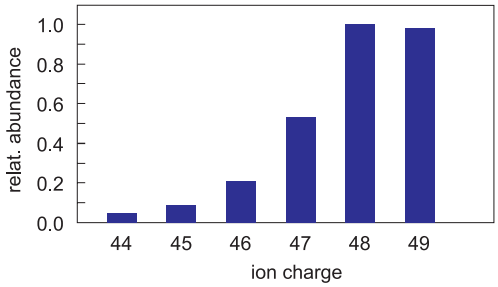

Fig. 5. Calculated ion charge state distribution of iridium ions inside the Dresden EBIT at an electron beam energy of E_e = 4 keV using a computer code described in [13].

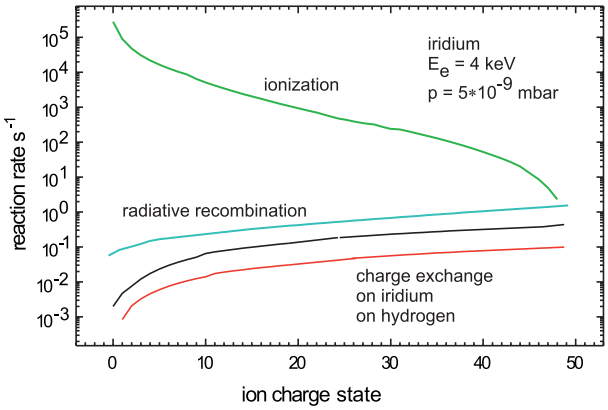

Fig. 6. Estimated reaction rates for the ionization of iridium ions at 4 keV electron energy and a pressure of 5×10^{-9} mbar in the trap.

A balance of estimated reaction rates at an electron energy of 4 keV and operation conditions typical during the experiment is given in Figure 6. The balance of the mentioned processes leads to an equilibrium ion charge state distribution after about 1 s ionization time. This behaviour is exemplarly shown in Figure 7 for an electron energy of 4 keV. As we have a constant current of iridium ions from the cathode there is a permanent flux into the trap region. For better ionization conditions a trapping time of 2 s has been chosen, *i.e.* a time where the charge state equilibrium is reached already. The permanent flux of low ionized iridium ions into the trap region is the reason that for all measured spectra contributions from lower ion charge states are present and deform the measured transition lines somewhat to the low-energy side of the spectra.

4 Radiative recombination

With the chosen operation parameters we derive krypton-like up to aluminium-like ions with small amounts of ions with charges to the neon-like sequence. Measured radiative recombination (RR)

$$\mathrm{A}^{q+} + e^- \rightarrow \mathrm{A}^{(q-1)+} + h\nu$$

spectra contain information on the derived ion charge states in the Dresden EBIT. In order to get the RR

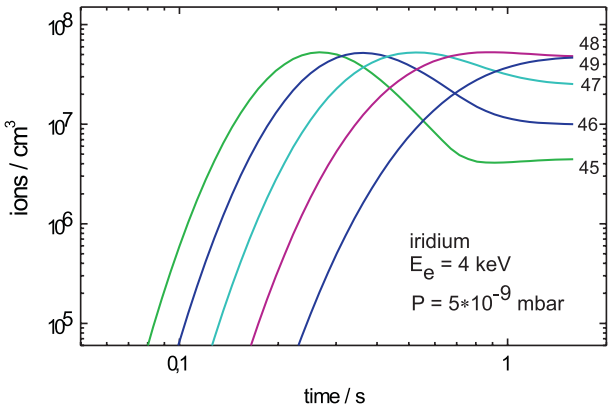

Fig. 7. Estimated reaction rates for the ionization of iridium ions at 4 keV electron energy and a measured pressure of 5×10^{-9} mbar in the trap.

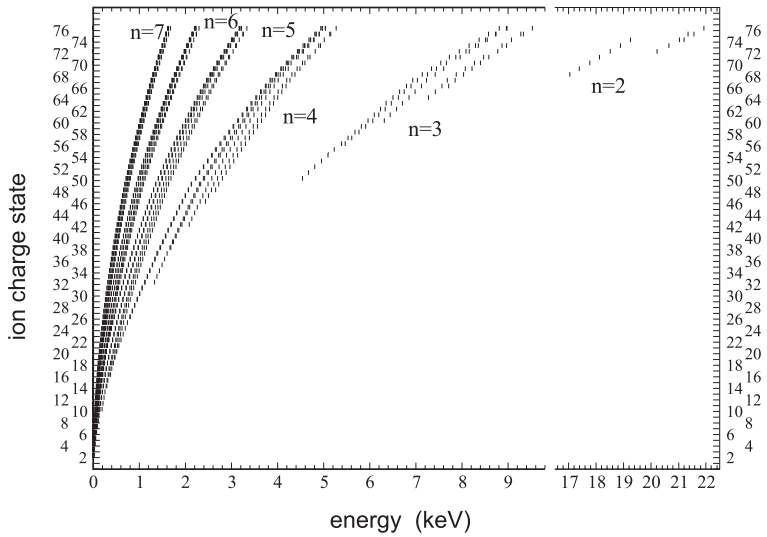

Fig. 8. Calculated radiative recombination energies for electron capture in the $n = 2$ to the $n = 7$ shells at different ion charge states q. The offset-energy is shown that must be added to the electron energy to get the line transition energies for radiative capture processes into different atomic subshells.

transition energies, Figure 8 shows calculated RR energies that must be added to the electron beam energies. It can be seen that radiative electron capture in shells with low principal quantum number leads to most significant energy shifts. Thus the signature for the capture into $n = 3$ subshells allows an analysis of the ion charge states existing in the EBIT electron beam. For capture into levels with higher principal quantum numbers the situation is more complicated because of the smaller energetic shifts of adjoining ion charge states. Line ensembles corresponding to the capture into different shells are energetically separated and can resolved with an energy-dispersive solid-state detector.

Measured X-ray spectra from radiative recombination processes are shown in Figures 9 and 10. Corresponding to the expected theoretical shifts of the transition lines in both figures an energy shift to higher energies with increasing electron beam energies can be observed. This behaviour coincides with the ionization threshold energies for the ionization of certain subshells as summarized in Table 2. Recombination capture into the $n = 3$ shells start at $E_e = 5$ keV and can be observed for all higher electron beam energies. The recombination capture into the $n = 2$ shell gives the clearest distinguished signature for different ionization stages as it is shown in Figure 8. Recombination into higher shells is characterized by closer energetic positions for recombination into adjacent ionization stages and into neighbouring ionic subshells.

In Figures 9 and 10 the common behaviour of the RR spectra is shown. Calculated line positions for capture into different ionic states are indicated. There exits a blend of ion charge states next to a certain mean ion stage. In Tables 3 and 4 calculated RR energies for all ion charge states between krypton-like and neon-like ions for the $n = 3$, 4, 5, 6 and 7 subshells are given. The calculations are done with a MCDF-code [12]. The RR energies must be added to the electron energy to derive the actual RR transition energy.

In Figure 11 a RR spectrum of nickel-like iridium ions at an electron beam energy of 10 keV is shown. A RR spectrum of predominantly argon-like iridium ions is shown in Figure 12. For the electron capture into $n = 3$ levels energetic positions of adjacent X-ray lines are indicated too.

Table 3. Calculated RR energies of iridium ion charge states from $q = 41$ (krypton-like ions) up to $q = 67$ (neon-like ions) for the $n = 3$, 4 and 5 subshells.

q	$3s$	$3p^-$	$3p$	$3d^-$	$3d$	$4s$	$4p^-$	$4p$	$4d^-$	$4d$	$4f^-$	$4f$	$5s$	$5p^-$	$5p$	$5d^-$	$5d$
41									1857	1834	1628	1622	1283	1231	1183	1100	1090
42								2083	1924	1895	1695	1686	1326	1274	1225	1145	1132
43								2139	1978	1953	1753	1746	1369	1317	1266	1185	1173
44								2201	2036	2010	1816	1805	1412	1360	1308	1228	1215
45								2258	2093	2058	1874	1864	1455	1404	1348	1269	1257
46							2435	2321	2157	2121	1940	1930	1501	1449	1392	1313	1301
47							2500	2378	2207	2182	2001	1995	1545	1491	1435	1357	1345
48						2656	2565	2442	2272	2246	2068	2062	1591	1538	1480	1402	1390
49						2722	2616	2491	2330	2304	2133	2126	1634	1583	1524	1447	1434
50					4540	2803	2698	2572	2417	2389	2228	2216	1687	1636	1576	1502	1488
51					4669	2884	2781	2651	2498	2470	2311	2302	1741	1690	1629	1555	1541
52					4806	2966	2864	2730	2580	2551	2398	2390	1795	1745	1681	1609	1595
53					4953	3049	2949	2810	2666	2635	2491	2479	1850	1800	1734	1664	1650
54					5093	3132	3034	2891	2754	2720	2582	2566	1905	1857	1788	1721	1705
55					5229	3215	3119	2972	2838	2797	2671	2648	1961	1913	1843	1777	1758
56				5466	5388	3302	3208	3062	2929	2890	2770	2748	2018	1971	1901	1836	1818
57				5608	5529	3388	3296	3143	3017	2976	2865	2840	2076	2030	1956	1894	1875
58				5765	5678	3475	3384	3230	3107	3068	2960	2940	2134	2089	2014	1953	1935
59				5910	5817	3563	3472	3314	3191	3156	3047	3034	2193	2148	2070	2011	1993
60			6315	6065	5962	3650	3562	3402	3288	3247	3153	3135	2251	2207	2129	2074	2054
61			6442	6195	6098	3738	3651	3487	3374	3336	3247	3231	2310	2267	2186	2132	2113
62			6581	6334	6234	3824	3741	3573	3467	3426	3348	3327	2370	2328	2245	2194	2173
63			6709	6467	6353	3911	3831	3653	3556	3515	3443	3422	2429	2389	2302	2254	2233
64		7273	6851	6620	6503	4002	3925	3744	3652	3610	3548	3526	2491	2452	2363	2318	2296
65		7422	6981	6746	6647	4092	4011	3833	3746	3705	3647	3629	2552	2512	2424	2381	2360
66	7711	7566	7120	6894	6795	4183	4105	3924	3842	3800	3752	3734	2614	2576	2485	2445	2423
67	7852	7681	7230	7033	6931	4268	4197	4013	3938	3894	3855	3836	2674	2639	2546	2509	2487

Table 4. Calculated RR energies of iridium ion charge states from $q = 41$ (krypton-like ions) up to $q = 67$ (neon-like ions) for the $n = 5$, 6 and 7 subshells.

q	$5f^-$	$5f$	$6s$	$6p^-$	$6p$	$6d^-$	$6d$	$6f^-$	$6f$	$7s$	$7p^-$	$7p$	$7d^-$	$7d$	$7f^-$	$7f$
41	1003	1000	835	807	781	737	731	685	684	588	571	556	529	526	498	497
42	1048	1043	866	838	812	768	761	716	714	611	594	578	552	548	521	519
43	1089	1085	897	869	841	797	791	746	744	634	617	600	574	570	543	542
44	1133	1129	928	900	872	828	821	777	775	657	640	623	597	593	566	565
45	1175	1171	960	931	902	858	851	807	805	681	664	646	619	615	589	587
46	1220	1216	992	964	933	890	883	840	837	705	688	670	643	639	613	611
47	1265	1262	1025	996	965	922	915	872	870	730	712	693	667	663	637	635
48	1312	1308	1058	1029	997	954	947	905	903	755	737	718	691	687	662	660
49	1358	1354	1091	1062	1029	987	980	938	936	779	762	742	716	712	686	685
50	1417	1410	1128	1099	1066	1025	1017	978	974	807	789	769	744	739	715	713
51	1470	1465	1166	1137	1103	1062	1054	1015	1013	835	817	797	771	767	743	741
52	1525	1521	1204	1176	1140	1100	1092	1054	1051	863	846	824	799	794	771	770
53	1584	1578	1242	1215	1178	1139	1130	1094	1091	892	875	852	828	823	801	799
54	1643	1635	1281	1254	1216	1179	1169	1135	1131	921	904	881	857	852	831	828
55	1700	1690	1321	1294	1255	1218	1207	1175	1170	950	933	909	887	880	861	857
56	1762	1752	1361	1335	1296	1259	1249	1218	1213	980	964	939	917	911	892	889
57	1823	1811	1402	1376	1334	1300	1289	1260	1254	1010	994	969	947	941	923	919
58	1884	1875	1443	1418	1376	1342	1331	1303	1298	1041	1025	999	978	972	955	951
59	1943	1936	1485	1460	1416	1383	1373	1345	1341	1072	1056	1029	1009	1003	986	983
60	2009	2000	1527	1502	1458	1427	1415	1391	1385	1103	1088	1060	1041	1034	1019	1016
61	2070	2063	1569	1545	1499	1468	1457	1434	1429	1135	1120	1091	1072	1066	1051	1048
62	2136	2125	1612	1588	1541	1512	1500	1480	1474	1167	1152	1123	1105	1098	1085	1081
63	2199	2189	1654	1631	1582	1555	1543	1524	1518	1199	1184	1154	1137	1130	1118	1114
64	2266	2256	1698	1676	1626	1600	1588	1571	1565	1232	1218	1186	1171	1163	1152	1149
65	2332	2322	1742	1720	1669	1645	1633	1617	1612	1264	1251	1219	1204	1196	1187	1183
66	2400	2390	1787	1765	1713	1691	1678	1665	1659	1298	1284	1252	1238	1230	1222	1219
67	2468	2458	1831	1811	1757	1737	1724	1713	1707	1331	1318	1285	1273	1264	1257	1254

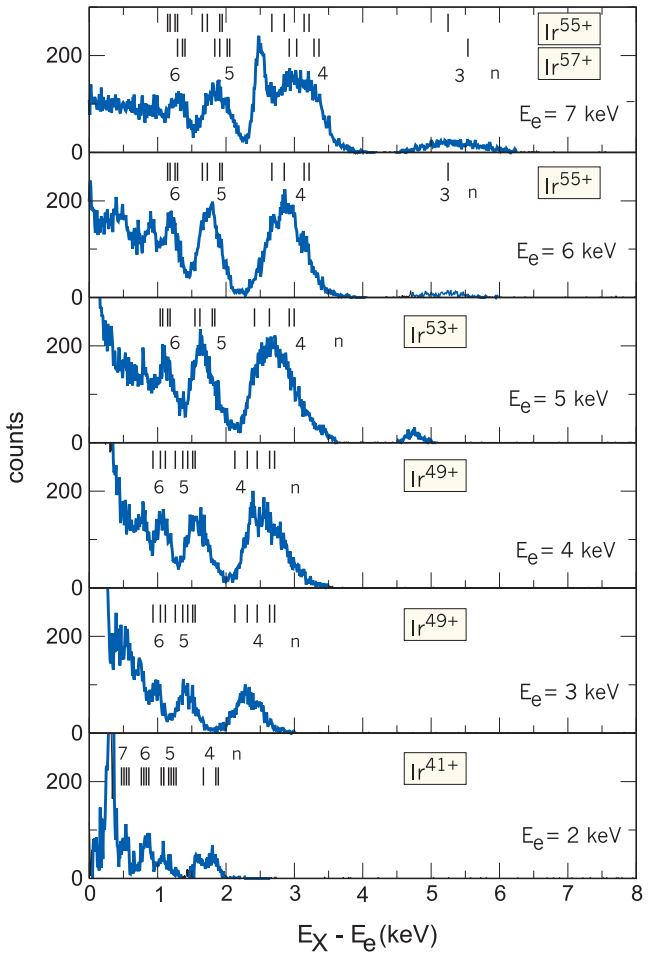

Fig. 9. Radiative recombination lines from different iridium ions at electron energies between 2 keV and 7 keV. Energetic positions of RR lines into different ions are indicated. All spectra are measured over the same time (2000 s) and under nearly equivalent vacuum conditions.

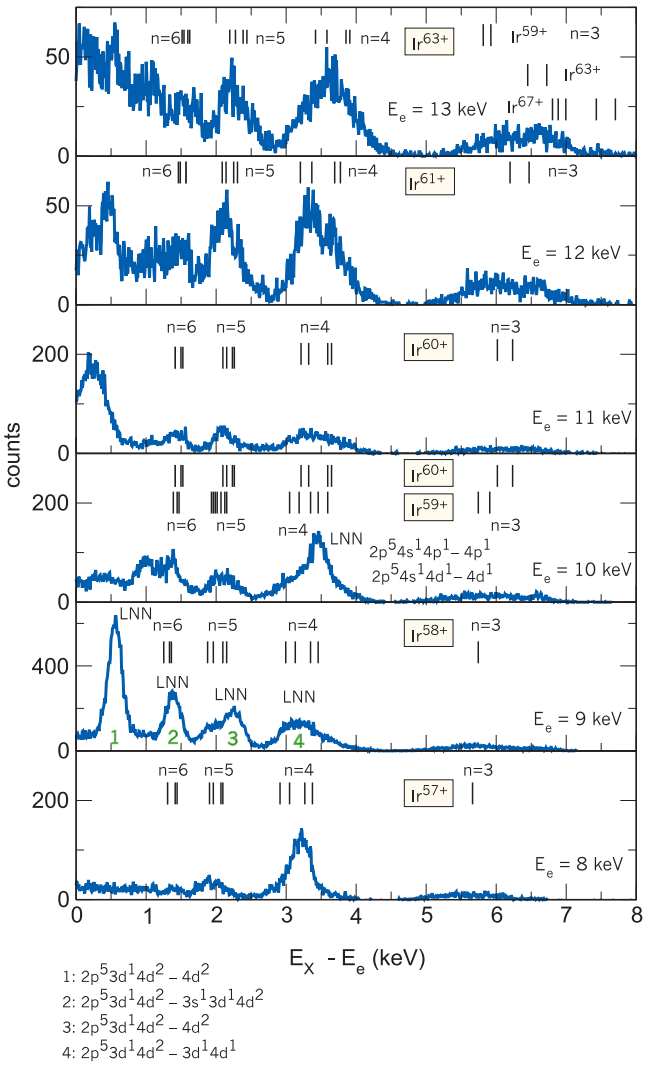

Fig. 10. Radiative recombination lines from different iridium ions at electron energies between 8 keV and 13 keV. Energetic positions of RR lines into different ions are indicated. For some DR transitions the main process is labeled. All spectra are measured over the same time (2000 s) and under nearly equivalent vacuum conditions.

RR energies of argon-like iridium are given for the $n = 3$, 4, 5, 6 and 7 subshells in Tables 3 and 4.

In Figure 13 the mean ion charge state derived from RR spectra of iridium ions is indicated as a function of the electron energy. The given results are mean ion charge states because there always exists a blend of different adjacent charge states. For $E_e = 2$ keV the dominant ions are krypton-like, for 4 keV we derive nickel-like ions, for 10 keV argon-like ions and for 13 keV silicon-like ions. The obtained ion charge states indicate clearly the role of radiative recombination and charge exchange processes in the ion trap. At the working pressure of 5×10^{-9} mbar for energies higher than 5 keV we do not reach the possible ionization stages if only the energetics of the actual ion ground state (see Tab. 2) is considered. From an energetic point of view neon-like iridium ions can be produced with 8 keV electron energy or higher. But in practice the derived ionization stages are somewhat lower. Nevertheless, experiments in the pressure region of about 1×10^{-9} mbar have shown, that it is possible to produce ions up to the neon-like sequence for energies higher than 8 keV.

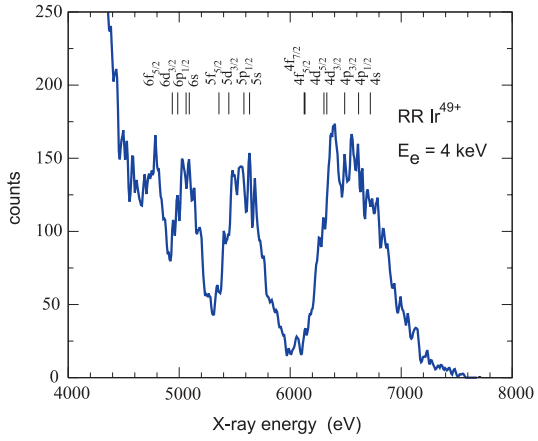

Fig. 11. Radiative recombination lines from nickel-like iridium ions at an electron energy of 4 keV.

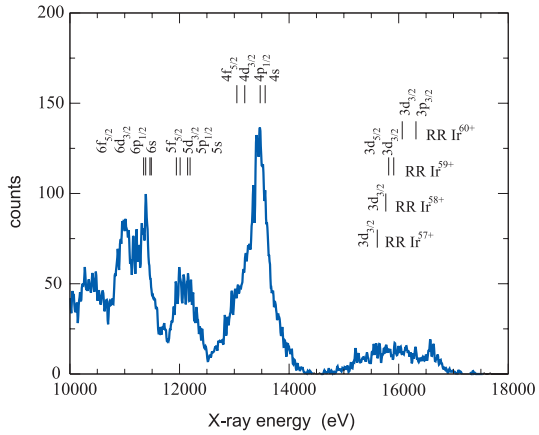

Fig. 12. Radiative recombination lines from argon-like iridium ions at an electron energy of 10 keV.

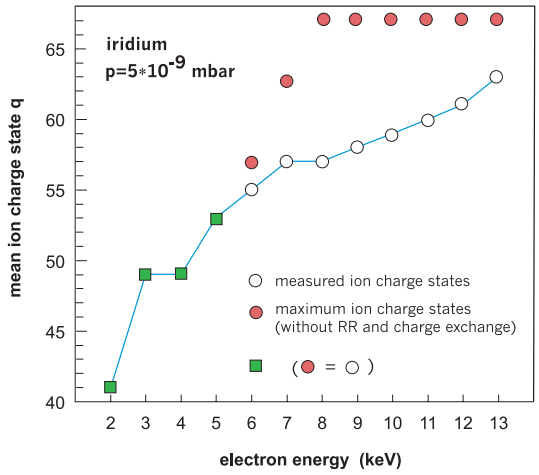

Fig. 13. Ion charge state q derived from the analysis of RR spectra at different electron beam energies E_e.

In Figure 14 X-ray spectra from direct excitation processes of $n = 2$ electrons and from RR processes at $E_e = 13$ keV are shown. In the upper part of Figure 14 the energetic line positions of Ir^{63+} indicate, that there are also contributions from adjacent ionization stages. To demonstrate this behaviour a modelled ion charge state distribution with the code mentioned above [13] is shown in Figure 15. The dominant ion charge state is Ir^{62+}, but with a high amount of Ir^{63+} ions. The dominant contribution to the uncertainty of the given calculation results is based on the fact, that the pressure around the electron beam in the drift tube section region is not known exactly. Nevertheless, to reach higher ion charge states the working gas pressure of the trap must be reduced in order to decrease charge reducing processes.

5 Conclusions

In the present work we demonstrate that with a room-temperature EBIT it is possible to provide X-ray spectroscopy of metallic ions over a wide range of ionic

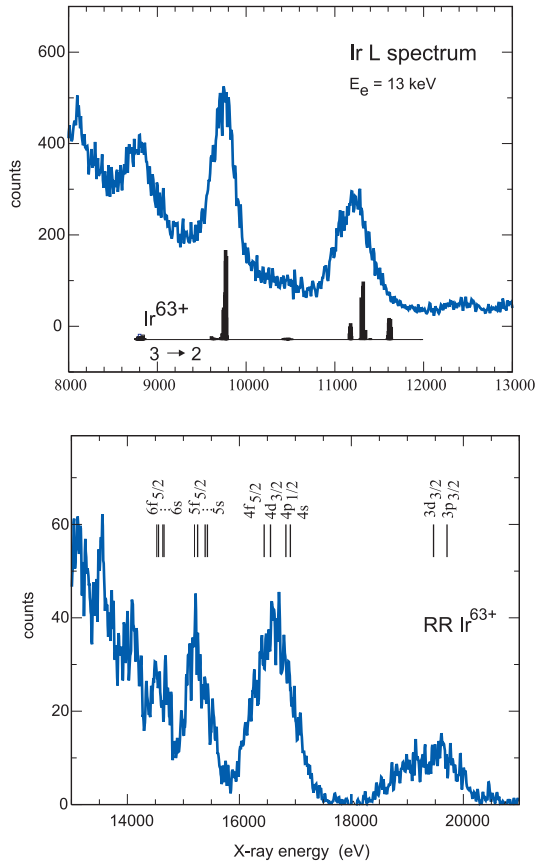

Fig. 14. X-ray spectra from direct excitation of $n = 2$ electrons and from RR processes at $E_e = 13$ keV.

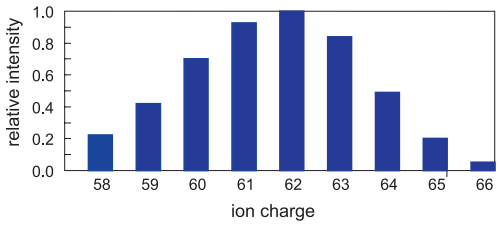

Fig. 15. Modelled ion charge state distribution for the spectra shown in Figure 14.

charge states. We firstly measured iridium X-ray spectra for different excitation conditions and analyzed selected spectra for radiative recombination and direct excitation processes. The measurements have shown, that model calculations can reproduce the actual ion charge state distribution in the electron beam in a sufficient way. With a room-temperature EBIT arises the possibility to investigate the ionization process in dense electron beams in dependence of the pressure over at least three orders of magnitude from 10^{-8} mbar up to 10^{-10} mbar. This opens up interesting possibilities to study ion production mechanisms under working conditions partially not available for cryogenic sources. Thereby the tuning of the electron energy allows to study processes which are of interest for different fields of research as nuclear fusion physics, astrophysics, ion source physics and others.

The work is supported by the EFRE fund of the EU and by the Freistaat Sachsen (Project 6937/1087) and by DFG (Project Zs 14/7-3). The authors would like to thank Dipl.-Phys. S. Landgraf and E. Steinhorst for their technical support during the experiments.

References

1. V.P. Ovsyannikov, G. Zschornack, Rev. Sci. Instrum. **70**, 2646 (1999).
2. V.P. Ovsyannikov, G. Zschornack, F. Grossmann, S. Landgraf, F. Ullmann, T. Werner, Rev. Sci. Instrum. **71**, 690 (2000).
3. V.P. Ovsyannikov, G. Zschornack, F. Grossmann, O.K. Kulthachev, S. Landgraf, F. Ullmann, T. Werner, Nucl. Instrum. Meth. Phys. Res. B **161**, 1123 (2000).
4. T. Werner, G. Zschornack, F. Grossmann, V.P. Ovsyannikov, F. Ullmann, Rev. Sci. Instrum. **71**, 2038 (2000).
5. `http://www.physik.tu-dresden.de/apg`
6. S.R. Elliot, P. Beiersdorfer, B.J. MacGowan, J. Nilson, Phys. Rev. A **52**, 2689 (1995).
7. A. Siminovici, D.D. Dietrich, R. Keville, T. Cowan, P. Beiersdorfer, M.H. Chen, S.A. Blundell, Phys. Rev. A **48**, 3056 (1993).
8. P. Beiersdorfer, A. Osterheld, S.R. Elliott, M.H. Chen, D. Knapp, K. Reed, Phys. Rev. A **52**, 2693 (1995).
9. S.R. Elliott, P. Beiersdorfer, M.H. Chen, Phys. Rev. Lett. **76**, 1031 (1996).
10. P. Mandelbaum, J.F. Seely, C.M. Brown, D.R. Kania, R.L. Kauffman, Phys. Rev. A **44**, 5752 (1991).
11. P. Beiersdorfer, S. von Goeler, M. Bitter, E. Hinnov, R. Bell, S. Bernabei, J. Felt, K.W. Hill, R. Hulse, J. Stevens, S. Suckewer, J. Timberlake, A. Wouters, M.H. Chen, J.H. Scofield, D.D. Dietrich, M. Gerassimenko, E. Silver, R.S. Walling, P.L. Hagelstein, Phys. Rev. A **37**, 4153 (1988).
12. I.P. Grant, B.J. McKenzie, P.H. Norrington, D.F. Mayers, N.C. Pyper, Comput. Phys. Commun. **21**, 207 (1980).
13. I.V. Kalagin, D. Küchler, V.P. Ovsyannikov, G. Zschornack, Plasma Sources Sci. Technol. **7**, 441 (1998).